Modification of wetting property of Inconel 718 surface by nanosecond laser texturing

Z. Yang [a,b,c], Y.L. Tian [a,b,c], C.J. Yang [a,b,*], F.J. Wang [a,b], X.P. Liu [c]

[a]School of Mechanical Engineering, Tianjin University, Tianjin 300350, China

[b]Key Laboratory of Mechanism Theory and Equipment Design of Ministry of Education, Tianjin University, Tianjin 300350, China

[c]School of Engineering, University of Warwick, Coventry CV4 7AL, UK

Corresponding author e-mail address: cjytju@tju.edu.cn (C.J. Yang)

Abstract

Topographic and wetting properties of Inconel 718 (IN718) surfaces were modified via nanosecond laser treatment. In order to investigate surface wetting behavior without additional post treatment, three kinds of microstructures were created on IN718 surfaces, including line pattern, grid pattern and spot pattern. From the viewpoint of surface morphology, the results show that laser ablated grooves and debris significantly altered the surface topography as well as surface roughness compared with the non-treated surfaces. The effect of laser parameters (such as laser scanning speed and laser average power) on surface features was also discussed. We have observed the treated surface of IN718 showed very high hydrophilicity just after laser treatment under ambient air condistion.And this hydrophicility property has changed rapidly to the other extreme; very high hydrophobicity over just about 20 days. Further experiments and analyses have been carried out in order to investigate this phenomena. Based on the XPS analysis, the results indicate that the change of wetting property from hydrophilic to hydrophobic over time is due to the surface chemistry modifications, especially carbon content. After the contact angles reached steady state, the maximum water contact angle (WCA) for line-patterned and grid-patterned surfaces increased to 152.3 ± 1.2° and 156.8 ± 1.1° with the corresponding rolling angle (RA) of 8.8 ± 1.1° and 6.5 ± 0.8°, respectively. These treated IN718 surfaces exhibited superhydrophobic property. However, the maximum WCA for the spot-patterned surfaces just increased to 140.8 ± 2.8° with RA above 10°. Therefore, it is deduced that laser-inscribed

modification of surface wettability has high sensitivity to surface morphology and surface chemical compositions. This work can be utilized to optimize the laser processing parameters so as to fabricate desired IN718 surfaces with hydrophobic or even superhydrophobic property and thus extend the applications of IN718 material in various fields.

Keywords: Inconel 718, Nanosecond laser, Surface morphology, Surface wettability, Surface chemical compositions

1. Introduction

As a precipitation-hardenable superalloy, IN718 has been widely used to make critical components of gas turbines, power plants, spacecraft and rocket motors due to its excellent corrosion resistance, thermal resistance, wear resistance and high strengths at elevated temperature [1-3]. However, IN718 is commonly classified as the difficult machining material because of high shear strength, low material removal rate and excessive tool wear by conventional machining methods [4]. Although it is reported that current hybrid manufacturing methods can pave a way to solve the aforementioned problems, there are many shortcomings such as high cost, long lead-time and environmental impacts that cannot meet the requirement for wide applications of IN718 material [5-6]. Thus it is urgent to seek alternative technique expanding the value of such material in potential applications.

Currently, extensive attention has focused on superhydrophobic surfaces that play a significant role in various applications related to energy, resources and environment, including self-cleaning, anti-fogging, anti-corrosion, anti-icing, anti- bacteria and drag reduction [7-17]. Superhydrophobic surface is generally defined as a solid surface with water contact angle (WCA) exceeding 150° and rolling angle (RA) below 10° [18, 35]. It is well-known that both surface topology and surface chemistry determine the wetting property of a particular solid surface. Therefore, surface wettability can be changed by surface roughness modification and by changing surface chemical component.

According to Wenzel model [19] and Cassie-Baxter model [20], surface roughness manipulation can contribute to improving hydrophobicity of the solid surfaces. In Wenzel model, it is assumed that a liquid droplet completely penetrates into the grooves

of rough surface. The contact angle θ_W can be modified by the following equation:

$$\cos\theta_W = r\cos\theta \quad (1)$$

Where r >1 is surface roughness parameter, θ represents contact angle for flat surface and is determined by the chemical compositions of surface layer. It can be deduced from the Eq. (1) that contact angle will decrease with increased roughness of a hydrophilic surface, whereas contact angle will increase when the roughness of a hydrophobic surface increases. Nevertheless, in most cases found in reality, the contact between a droplet and a rough surface is never complete. Indeed, air pockets are trapped in the grooves, which leads to Cassie-Baxter model with a composite interface. The contact angle θ_{CB} on such surfaces is given as follow:

$$\cos\theta_{CB} = r_f f\cos\theta + f - 1 \quad (2)$$

For Cassie-Baxter model, the key factors affecting contact angle value are the roughness parameter of wetted area r_f, the portion of surface wetted by testing liquid f and the chemical compositions of surface layer, associated with θ [21]. Therefore, according to Eq. (2), one can modify θ_{CB} on the rough surface by simply varying surface morphology and, as a result, the portion of wetted solid area f. Theoretically, a superhydrophobic surface can be achieved on any intrinsically hydrophilic materials [22-24].

Inspired by wetting model and the famous “lotus effect” with self-cleaning property, researchers have fabricated artificial superhydrophobic surfaces by the combination of two important factors: micro/nanoscale hierarchical structures and low surface energy substances. Based on the basis of such principle, a variety of methods have been employed to obtain thermodynamically stable hydrophobic or even superhydrophobic surfaces through controlling both of the surface chemical components and surface morphological structures, such as sol-gel coating [25-26], electrochemical deposition [27], chemical etching [28], laser surface texturing [29-31] and spray-coating [32]. Among these options, laser treatment is a promising technique to create superhydrophobic surfaces [33].

According to previous literatures, surface wettability can be modified to exhibit hydrophobic or superhydrophobic property by laser treatment followed by surface

chemical modification. Boinovich [34] reported that nanosecond laser treatment with additional surface modification of low surface energy fluorooxysilane was employed on aluminum alloy to fabricate superhydrophobic surfaces, with the WCA of 173.4 ± 1° and RA of 2.4 ± 1.2°. The results showed that laser texturing used to create multimodal roughness may be simultaneously used for modifying the physicochemical property. Compared to one-fold laser treatment, the intensive laser treatment resulted in the formation of an oxide surface layer with better barrier property for transfer of water molecules. Similarly, the reed leaf-like superhydrophobic surfaces [35] was obtained on stainless steel by UV nanosecond laser direct writing with subsequent fluorooxysilane modification. By controlling laser parameters of laser powers and laser scanning intervals, three typical microstructures including flat microstructure, micro-grating tructure and biomimetic hierarchical mico/nanostructures were obtained. As a result, the fabricated biomimetic structures revealed excellent superhydrophobicity with a WCA of 157 ± 1°and RA of 1 ± 0.5°. Emelyanenko [36] also fabricated superhydrophobic surfaces on stainless steel but using IR ytterbium fiber laser treatment with subsequent coating of fluorooxysilane. The fabricated surfaces exhibited chemical stability on long-term contact angle with water and remarkable water repellency, with the WCA of 170.9 ± 2.2° and RA of 1 ± 0.5°. Milionis [37] studied the development of magnetic nanocomposite PDMS sheets with superhydrophobic surfaces generated by UV nanosecond laser pulses. The laser treatment induced chemical and structural changes to the surface of the composites, which contributed to superhydrophobicity. Besides, the investigation of the laser pulses indicated that the exposure to increasing the number of laser pulses enhanced considerably the surface roughness as well as the surface wettability.

Nevertheless, by direct laser treatment with no additional silanization coating, many scholars have successfully modified surface wettability to obtain hydrophobic or superhydrophobic samples. Directly after laser treatment, the surfaces showed hydrophilic behavior but gradually became hydrophobic or superhydrophobic property over time. The time evolution of wettability is usually attributed to the change of surface chemical compositions. For example, Ta [38] investigated the wetting behavior on

nanosecond laser patterned copper and brass surfaces. The results showed that laser treated surfaces exhibiting WCAs above 152° with contact angle hysteresis around 3-4° have been achieved. It was claimed that the variation in wetting property was ascribed to the partial deoxidation of oxides on the surface induced during the laser ablation. However, Boinovich et al. [39], who commented Ta's paper, proposed that the adsorption of airborne hydrocarbon contaminations on the laser treated surface would be another reason for achieving the superhydrophobic state. Inspired by previous research, laser processing is a facile, non-contact, relatively inexpensive and very accurate manufacturing method [40]. Hence it has been widely employed to produce many micro holes, cones and even complex patterns on a broad range of materials. In this work, nanosecond laser with high power was applied to manufacture the difficult machining material of IN718.

To the best of authors' knowledge, few scientific reports concentrated on surface wettability of IN718 material so far. This work is an attempt to investigate the effects of surface patterns and surface chemistry on surface morphology and wetting property of IN718 by nanosecond laser treatment without further chemical coating. Firstly, laser-inscribed microstructures (i.e. line, grid and spot pattern) with various distance between successive grooves or holes were fabricated on prepared samples. We also discussed the influences of laser parameters on surface morphology. Then surface roughness, SEM images and 3D profiles of the sample surfaces were measured so as to characterize surface morphology. We also confirmed the steady wetting property of the as-prepared IN718 surfaces by WCA and RA measurements. Finally, the surface chemical compositions were analyzed by XPS and the hypothesized explanations for the noticed change of WCAs were proposed.

2. Experimental

2.1. Material details

The base material used in this investigation was IN718, the chemical composition of which is given in Table 1. The bar of IN718 was firstly cut by wiring electronic discharge machining (WEDM) and then mechanically polished to a surface roughness (R_a) of 1.02 μm. Prior to being subjected to laser irradiation, the polished samples with

a size of Φ20 mm × 1 mm were cleaned by a 5 minutes ultrasonic bath in acetone and followed by a 5 minutes ultrasonic bath in ethanol.

2.2. Nanosecond laser irradiation

After the metallographic preparation, various microstructures were fabricated on IN718 surfaces by laser irradiation using the Ytterbium nanosecond pulsed fiber laser system (IPG photonics from Germany). The parameters of the laser system are shown in Table 2.

Table 1 Chemical composition of IN718

Elements	Ni	Nb	Cr	P	S	Si	C	Mn
wt. (%)	53.16	5.48	18.03	0.015	0.002	0.16	0.07	0.08
Elements	Al	Co	TAt	B	Cu	Ti	Mo	Fe
wt. (%)	0.66	0.23	0.008	0.0028	0.07	1.15	3.11	balanced

Table 2 Laser system parameters

Wavelength (nm)	Average power (W)	Pulse duration (ns)	Repetition rate (kHz)	Spot diameter (μm)	Fluence (J/cm^2)
1064	0-20	50	20	60	0-35.38

The polished samples placed on the working platform were irradiated by the moving laser beam. As a result, the grooves or holes were produced on their surfaces by the raster scanning of laser beam. Figs. 1(a) and (b) show the line pattern was formed when laser beam began at the start point, with a zigzag scanning path, stopped at the end point. As shown in Fig 1(c) and (d), the grid pattern was obtained if the laser trace then rotated through 90° to scan by the same path. Additionally, according to the laser scanning strategy shown in Fig. 1(e), the spot pattern with many holes was established on the surface of IN718 shown in Fig. 1(f). Each hole was formed by many laser pulses irradiation. The number of pulses N could be calculated by the following equation [30]:

$$N = \frac{\pi \Phi f}{4V} \tag{3}$$

Where Φ and f are laser spot diameter and repetition rate, respectively. V is the laser scanning speed. Based on the parameters in Table 2 and 3, each hole was produced

by 18 laser pulses irradiation. After laser treatment, surface morphology was determined by surface pattern and the distance between the successive grooves and holes. Besides, the profile of the ablated grooves and holes had a high affinity for laser parameters such as laser scanning speed and average power. Five groups of experiments (presented in Table 3) were carried out using the single variable method to comprehensively investigate the effects of surface patterns (Group 1-3) and laser parameters (Group 4-5) on nanosecond-laser-inscribed surface morphology and wettability of IN718 material. The whole irradiated area on all samples surfaces was confined as a square with the size of 10 mm×10 mm. Laser irradiation experiments were performed in air under the atmospheric conditions.

2.3. Surface measurement and characterization

The effects of laser treatment on surface morphology were studied by means of SEM (FEI, Quanta 250 FEG). A white light confocal microscope (Zeiss CSM700) was used to measure surface average roughness (R_a). Groove depth and width as well as 3D profile of the samples were measured by a laser confocal scanning microscope (Olympus, LEXT-OLS4000). The contact angles were measured by sessile drop technique using a 3 μL distilled water droplet at the room conditions of the constant temperature 25℃ and air humidity around 50%. The contact angles were recorded when the dispensed droplet reached the equilibrium state on the surfaces. For the needs of date reliability and result reproducibility, at least five different locations were measured on each sample to determine the surface roughness and contact angle.

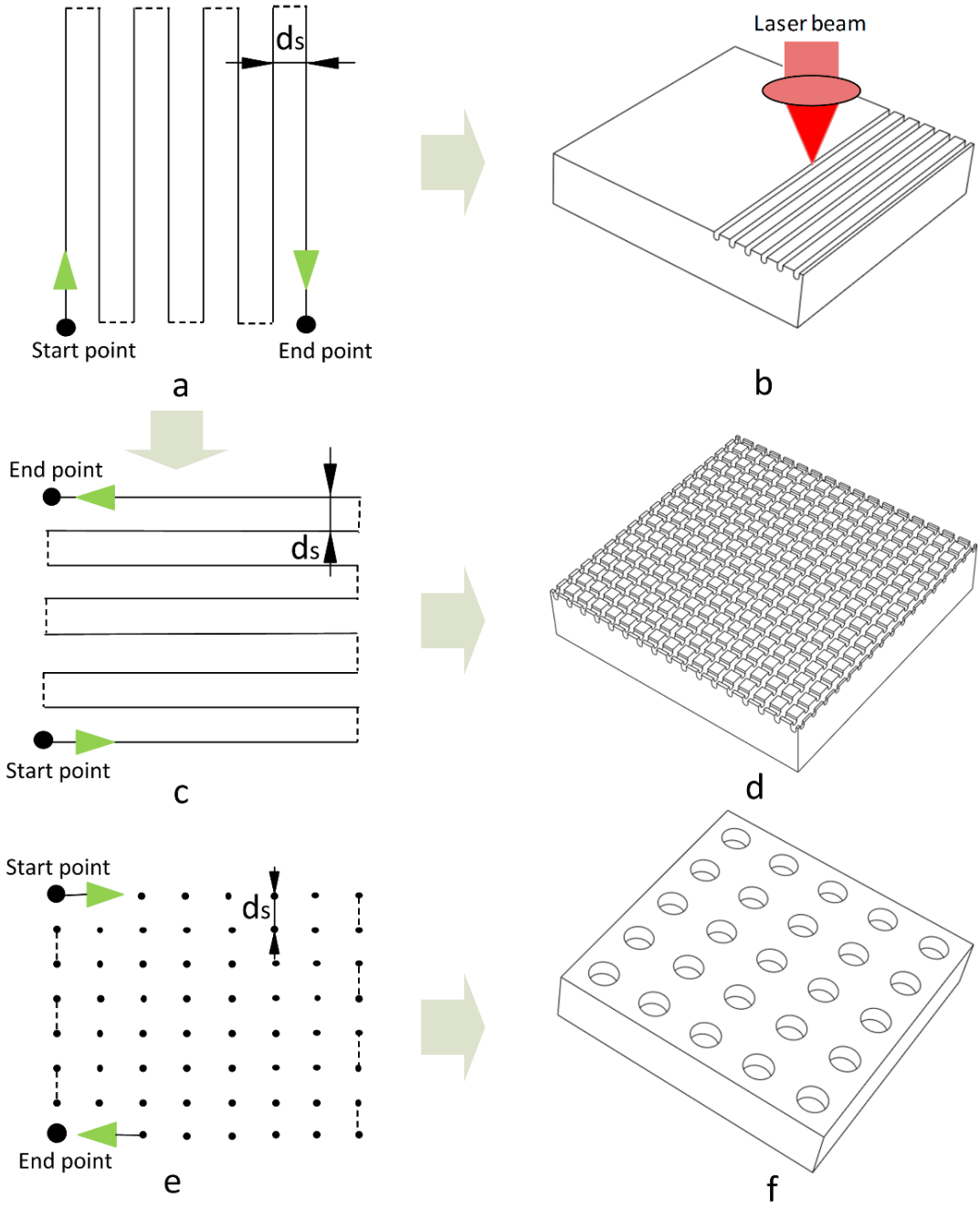

Figure 1. Schematic explanation of laser performance for producing grooves or holes on IN718 surface. (a), (c) and (e) were the path of laser beam from the top view. (b), (d) and (f) were sample surfaces after laser irradiation with line pattern, grid pattern and spot pattern, respectively.

Table 3 Important experimental details for each group of laser treatment

Treatment	Surface pattern	Laser power (W)	Scanning speed (mm/s)	Laser beam distance d_s (μm)
Group 1	line	10	50	50,60,70,80,90,100
Group 2	grid			
Group 3	spot			
Group 4	line	10	20,30,40,50,60,70	80
Group 5	line	4,8,10,12,16	50	

3. Results and discussion

3.1. Analysis of surface morphology

The surface topographic characterization clearly illustrated the effect of laser ablation on the surface morphology of IN718 material. Evidently, the modified surface morphology varied when different laser processing strategies were performed on the prepared samples. In this section, SEM and 3D confocal images of the laser ablated surfaces are comprehensively discussed to investigate the effects of various laser-inscribed patterns and laser parameters on surface morphology.

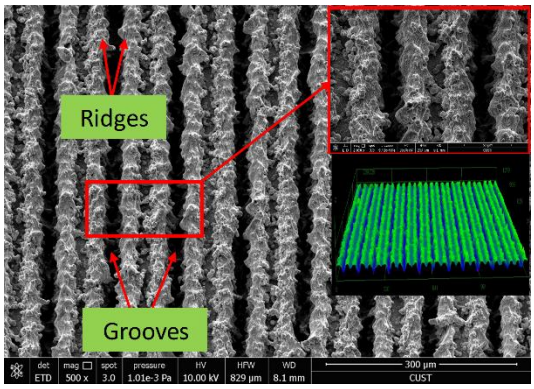

(a) Line pattern

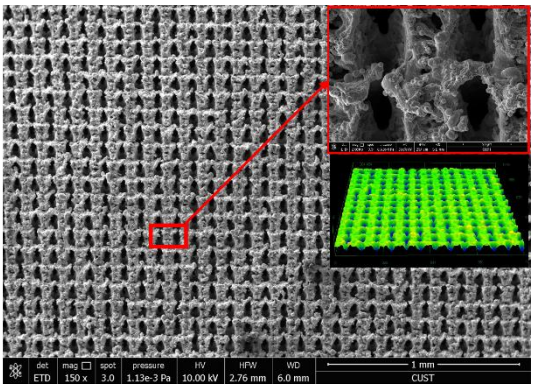

(b) Grid pattern

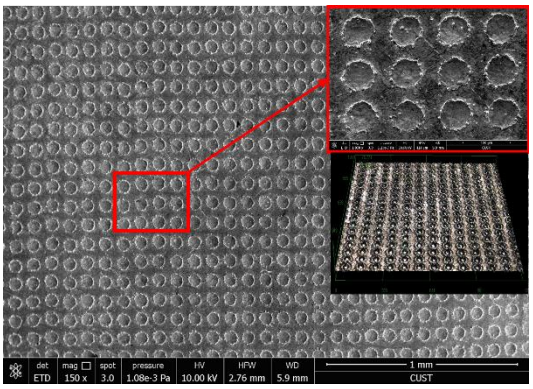

(c) Spot pattern

Figure 2. SEM images of different surface micropatterns: (a) Line pattern (b) Grid pattern (c) Spot pattern. The insets are corresponding magnified SEM and 3D confocal images.

3.1.1. Effect of laser-inscribed patterns on surface morphology

After laser treatment, three types of microstructures were fabricated on IN718 surfaces, and their corresponding surface SEM images and 3D profiles are shown in Fig. 2. The width and depth of the laser ablated grooves for line pattern (except the sample with distance of 50 μm) are 33 ± 4.6 μm and 23 ± 2.9 μm, respectively. It is clearly noted that the IN718 surfaces underwent the processes of melting, splashing and freezing in sequence. Also, we can see that the debris (i.e. redeposited materials) was covered by large numbers of micro and nanoscale particles, which can alter surface morphology in comparison to the pristine polished surfaces. This is probably caused by rapid cooling and solidification of splashing material. This phenomenon can be specially observed from the surface with spot pattern as shown in Fig. 2(c). However, the diameter and depth of the laser ablated holes for spot pattern are 48 ± 1.3 μm and 4 ± 0.5 μm, respectively. Among these three patterns, the surfaces with grid pattern had the greatest impact on surface morphology since this kind of structure (Fig. 2(b)) was the most complicated one and the proportion of laser ablated area was the largest.

Besides, the distance between successive grooves or holes also influenced the surface morphology. In this study, the distance was set to be 50, 60, 70, 80, 90 and 100 μm, respectively. Previous literature reported that the changes of surface morphology would become more distinct with the decrease of distance [41]. In order to check this

conclusion, surface roughness of the samples was measured using a white light confocal microscopy.

According to Table 4, it is confirmed that the grid pattern experienced the most serious laser ablation because the values of surface roughness for grid pattern were relatively higher than that for line pattern. The surfaces with spot pattern exhibited the minimum roughness values, which meant that this micro/nanostructure had the smallest impact on surface morphology. The reasons may lie in less molten materials resolidified on the brim of laser ablated holes, and a large presence of untreated surface was visible as shown in Fig. 2(c).

Table 4 Surface roughness of patterned samples with various distance

Distance (μm)	Surface roughness R_a (μm)		
	Line pattern	Grid pattern	Spot pattern
50	12 ± 1.6	16 ± 2.5	7 ± 0.9
60	8 ± 0.9	11 ± 2.1	5 ± 0.6
70	13 ± 1.3	19 ± 1.7	9 ± 0.8
80	16 ± 1.2	20 ± 1.9	4 ± 0.5
90	17 ± 0.8	25 ± 1.2	4 ± 0.4
100	17 ± 0.9	26 ± 1.6	3 ± 0.3

However, it can be found, with the increase of distance, that surface roughness did not show a downward trend as described in previous investigation [41] but presented an earlier decrease and later increase trend on the whole. In this study, we propose two main reasons to elucidate the discrepancies. On the one hand, it is perhaps attributed to the high laser power that led to the absence of ripple structures normally found on the laser ablated surface. The high magnification picture (Fig. 3(a)) shows that, when the laser beam with higher power was performed on the surfaces, the huge amount of thermal energy accumulated at a localized region and the melting material may slightly move to form layer-by-layer structures before resolidification. The arbitrary accumulation of this kind of structure made the surface more rough, particularly for smaller distance. On the other hand, the high laser power resulted in remarkable depth

of the groove, but no distinct grooves were observed on laser ablated surface when the laser beam with the smallest distance of 50 μm as shown in Fig. 3. This is because the diameter of laser beam was greater than the interval width of grooves or holes, which resulted in overlapped section (shown in Fig. 4). In this paper, the redeposited materials covered on the brim of untreated zone are termed as ridges. Due to the small interval of laser beam, the existing overlapped section would make wavy structures and there were no distinct grooves on the laser treated surface, which could be verified by Fig. 3(b). As a result, the forest of entangled and compacted microstrcutures made the surface with the distance of 50 μm much rougher than the one with the distance of 60 μm. With the growth of distance, the overlapped effect lessened and the treated surface exhibited evident grooves as shown in Fig. 2(a). Consequently, the roughness value then increased when the distance went up in our experiment.

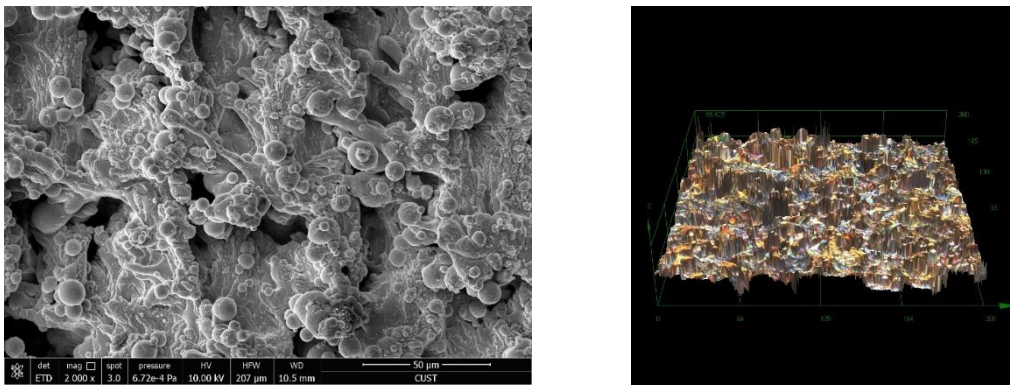

(a) (b)

Figure 3. High magnification SEM image (a) and 3D profile (b) of line pattern with distance of 50 μm.

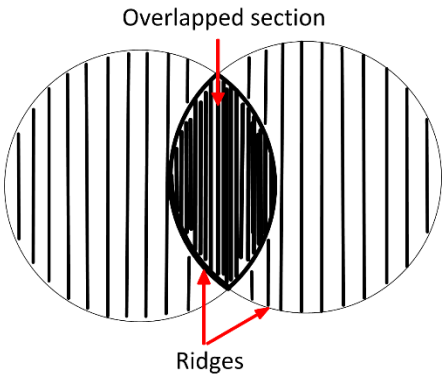

Figure 4. Schematic explanation of overlaps between successive grooves

3.1.2. Effect of laser scanning speed on surface morphology

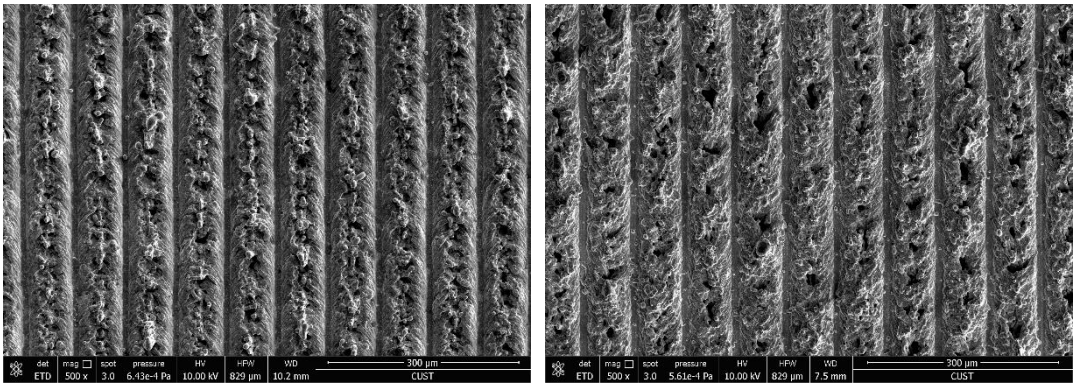

(a) (b)

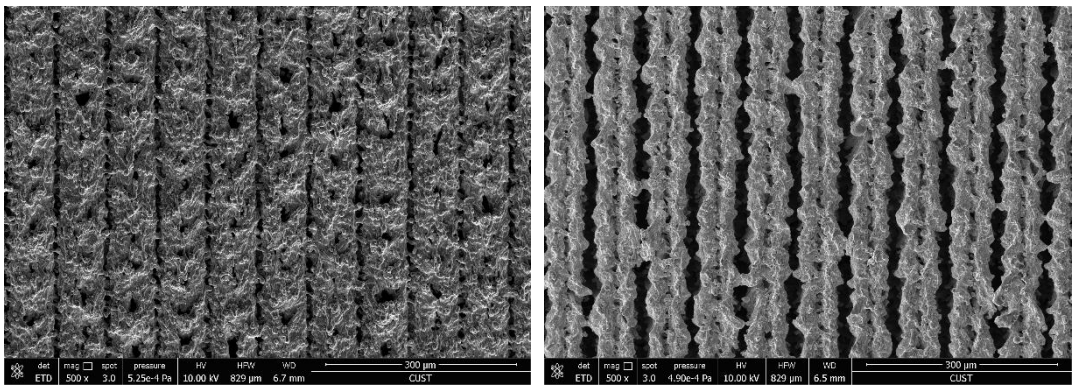

(b) (d)

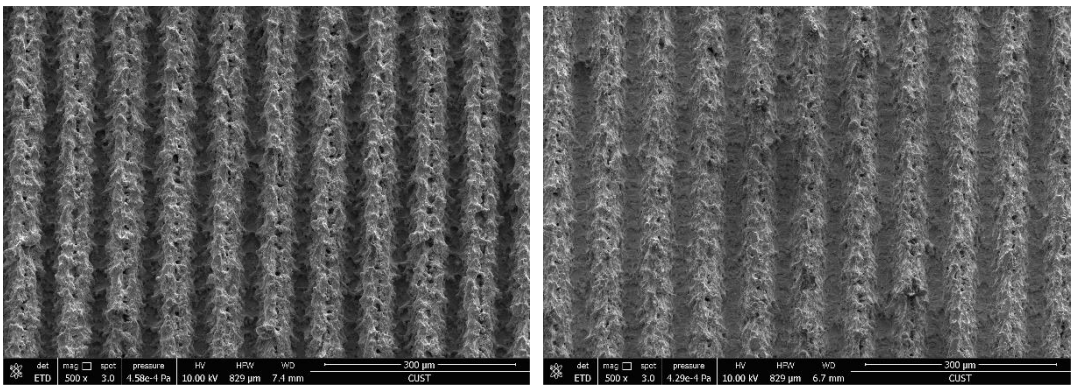

(e) (f)

Figure 5. SEM images of surface structures with various laser scanning speed: (a) 20 mm/s (b) 30 mm/s (c) 40 mm/s (d) 50 mm/s (e) 60 mm/s (f) 70 mm/s

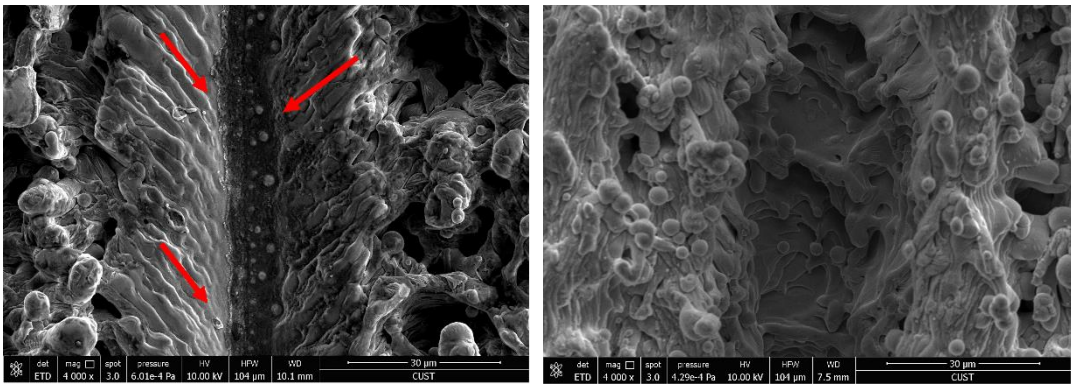

(a) (b)

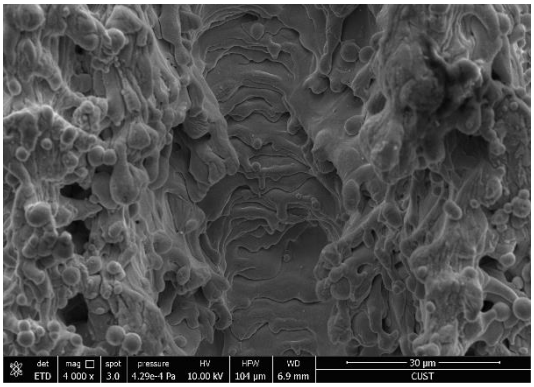

(c)

Figure 6. High magnification SEM images of surface structures with laser scanning speed: (a) 20 mm/s (b) 50 mm/s (c) 70 mm/s

Fig. 5 shows SEM images of surface structures under different laser scanning speed. With the increase of laser scanning speed, surface morphology changed significantly, which was caused by different number of pulses preformed at per unit lengths of the groove. Due to more laser pulses, low scanning speed led to more molten materials and smaller particles on the resolidified materials. The molten materials could easily move into the fabricated grooves and resolidified in the bottom (along the direction of the red arrow shown in Fig. 6(a)). This is the reason why the depth of groove was smaller for laser scanning speed 20 mm/s than that for 50 mm/s. When the speed went up further to 70 mm/s, less number of pulses was performed at per unit of the groove. Hence, the depth of groove decreased for high scanning speed. However, the width of the grooves for various scanning speed witnessed little change in this experiment. It is interesting to note that with the increasing of laser scanning speed,

there were more cracks created on the bottom of the ablated grooves. The reason for this phenomenon could be related to the effect of thermal expansion and cold contraction. The high laser scanning speed resulted in severe such effect, so more cracks and particles would be produced in the laser ablated area. On the whole, when the laser scanning speed was 50 mm/s, the surface morphology was changed the most degree, which could be verified in Table 5.

Figs. 5, 6 and Table 5 indicated that laser scanning speed had a great impact on surface morphology and surface roughness due to the factors of groove depth and width as well as the thermal expansion and cold contraction effect. In order to fabricate optimum laser-inscribed surface with best wetting property, laser scanning speed should be set rationally.

Table 5 Details of surface structures created by various laser scanning speed

Laser scanning speed (mm/s)	Groove width (μm)	Groove depth (μm)	Roughness R_a (μm)
20	35 ± 3.1	18 ± 1.2	8 ± 1.8
30	36 ± 2.9	20 ± 1.3	9 ± 1.5
40	35 ± 4.2	21 ± 2.2	13 ± 1.2
50	33 ± 4.6	23 ± 2.8	16 ± 1.4
60	33 ± 3.8	19 ± 1.3	13 ± 0.9
70	35 ± 3.2	15 ± 1.8	11 ± 0.6

3.1.3. Effect of laser average power on surface morphology

Apart from laser scanning speed, laser average power is another important factor influencing the surface topology. Corresponding SEM pictures and surface data of laser ablated area are shown in Figure 7 and Table 6, respectively.

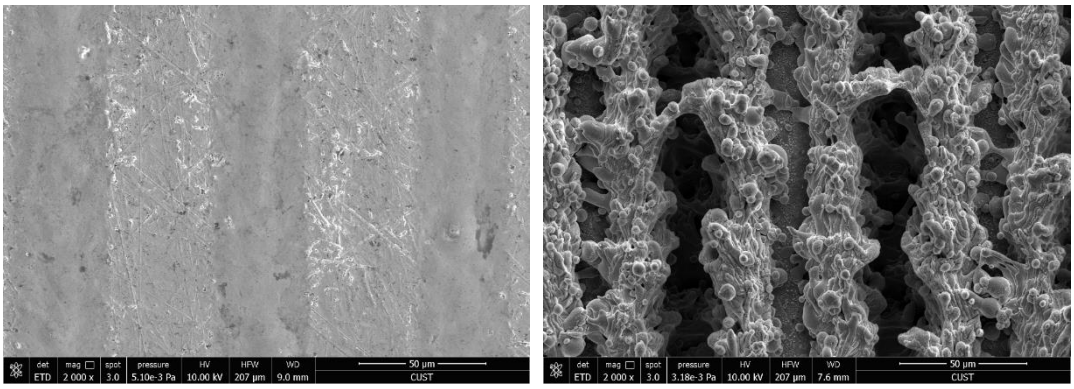

(a) (b)

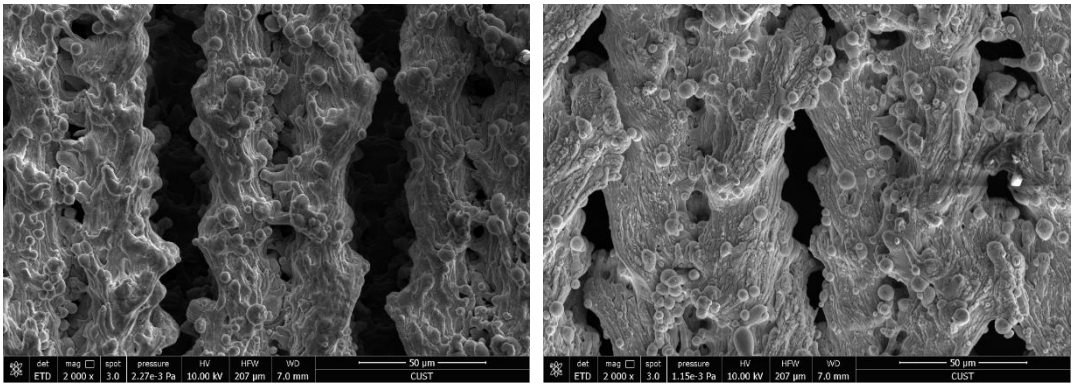

(b) (d)

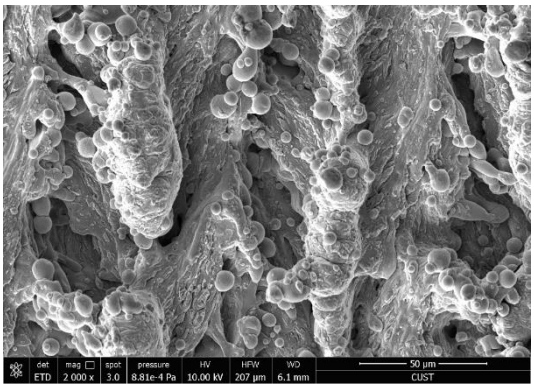

(e)

Figure 7. SEM images of surface structures with various laser average power: (a) 4 W (b) 8 W (c) 10 W (d) 12 W (e) 16 W

Table 6 Details of surface structures created by different laser average power

Laser average power (W)	Groove width (μm)	Groove depth (μm)	Roughness R_a (μm)

4	38 ± 1.2	5 ± 0.5	1 ± 0.6
8	35 ± 2.8	16 ± 1.5	11 ± 1.1
10	33 ± 4.6	23 ± 2.9	16 ± 1.3
12	-	-	15 ± 0.9
16	-	-	11 ± 1.0

As can be seen from Fig. 7(a) that when laser average power was set at 4 W, very few materials redeposited on the edges of laser ablated grooves and the depth of the grooves were much smaller in comparison to higher laser power. Also, a large amount of untreated IN718 surface was visible in this case. It can be inferred that the lower laser average power resulted in slight changes of surface morphology, which also can be verified by the smallest surface roughness value of 1 ± 0.6 μm as shown in Table 6. With the increase of the laser average power (8 W and 10 W), the width of the laser ablated groove witnessed a slight decrease. However, the depth of the laser ablated grooves deepened. Especially, when laser power was 10 W shown in Fig. 7(c), the large volume of splashed molten materials resolidified on the untreated area and almost covered the whole untreated surface, which resulted in a rougher surface. It also can be proved from the largest roughness value of 16 ± 1.3 μm shown in Table 6. However, it is not meant that the higher laser average power, the rougher surface can be obtained. Fig. 7(d) and (e) show that when laser power was set at 12 W and 16 W, the molten materials would slightly move before resolidification. So the width of the grooves would diminish as well as the surface roughness value. The reason of above mentioned phenomenon might be that more material would be ablated from the groove and then cover the previous groove at higher laser average power. As a result, there were no grooves formed on the as-prepared surfaces.

It also can be deduced from Fig. 7 and Table 6 that laser average power had a great impact on surface morphology and surface roughness. In order to obtain surface with desired property, the laser average power also should be optimized.

3.2. Analysis of surface wettability

The wettability of IN718 surfaces was investigated by WCA and RA. Fig. 8 shows

the process of WCA measurement. A 3 μL droplet of distilled water was placed on the untreated and laser treated samples surfaces in air at atmospheric conditions. Then a side view of droplet was automatically captured and calculated by the installed software as shown in Fig. 9. Before and after laser treatment, the WCA of polished IN718 sample surface was measured every day and the mean value was 45.2° with the standard deviation of 0.6°. Directly after laser irradiation, the WCA witnessed a considerable change over time. The investigation of the influence of surface patterns on surface wettability has been presented as follow:

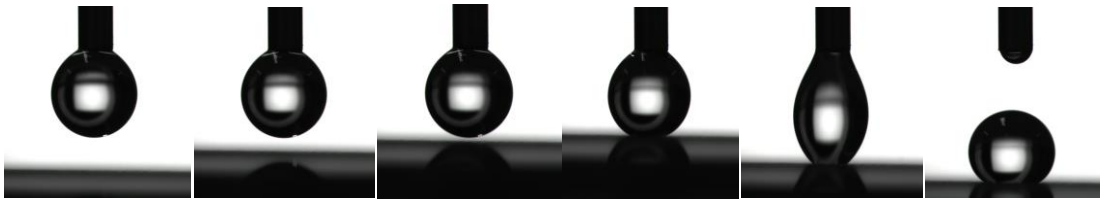

Figure 8. The process of placing the distilled water droplet

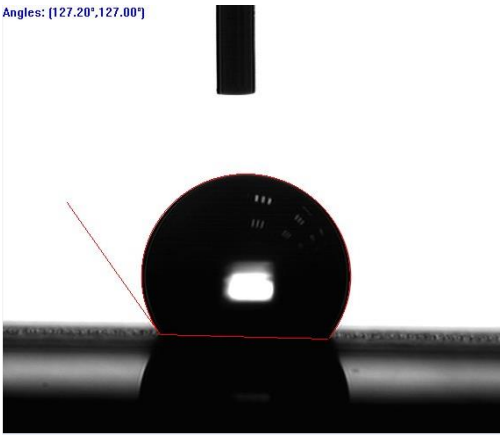

Figure 9. Contact angle measurement

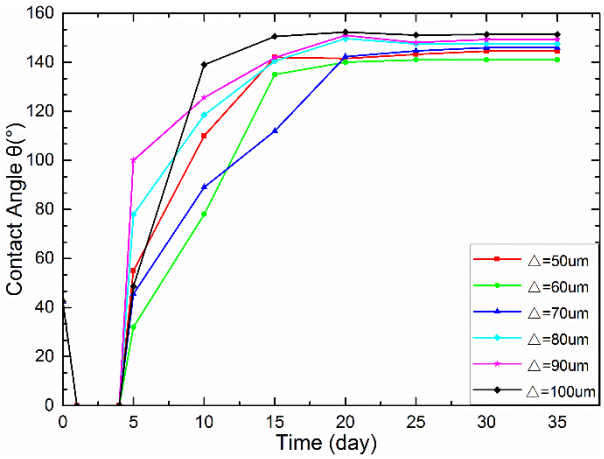

(a)

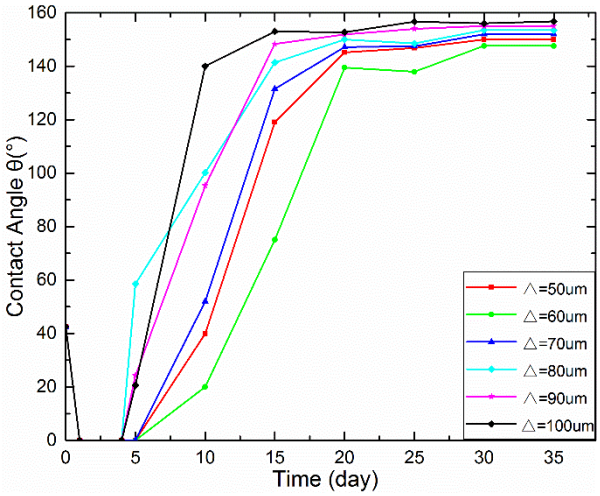

(b)

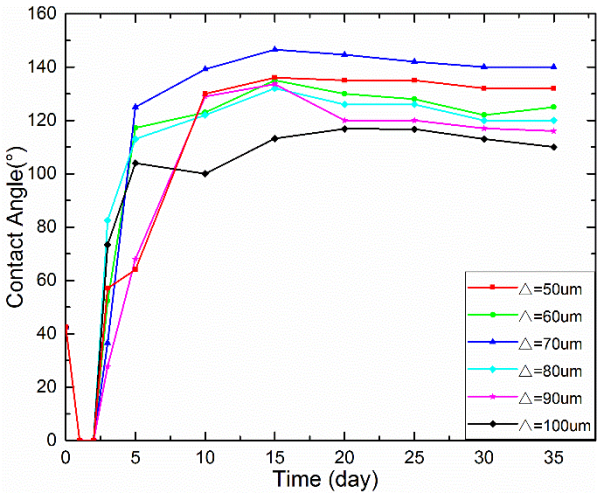

(c)

Figure 10. Evolution of contact angle over time for (a) line pattern (b) grid pattern (c) spot pattern

Table 7 Average apparent contact angle and rolling angle of the treated surfaces

Distance	Line pattern		Grid pattern		Spot pattern	
(μm)	WCA (°)	RA (°)	WCA (°)	RA (°)	WCA (°)	RA (°)
50	144.5 ± 1.1	23.5 ± 1.5	150.6 ± 0.9	9.7 ± 1.2	132.3 ± 3.6	43 ± 5.6
60	141.6 ± 0.8	28.2 ± 1.3	147.7 ± 1.3	15.6 ± 0.9	125.5 ± 5.2	65 ± 4.3
70	146.1 ± 1.2	19.6 ±	152.6 ± 0.8	8.5 ± 1.0	140.8 ± 2.8	36 ± 6.1

		1.6				
80	147.6 ± 0.9	15.7 ±	153.5 ± 1.0	7.6 ± 1.1	120.9 ± 4.6	70 ± 8.2
		2.2				
90	149.3 ± 1.0	12.6 ±	155.3 ± 0.8	7.3 ± 1.3	116.6 ± 5.3	-
		1.8				
100	152.3 ± 1.2	8.8 ± 1.1	156.8 ± 1.1	6.5 ± 0.8	110.3 ± 5.6	-

It is essential to understand the effect of microstructures with respect to the contact angles. Fig. 10 depicts the evolution of WCAs as a function of time for three types of surface patterns. Table 7 presents the stable WCAs and the corresponding RAs.

Time dependency of WCA for line-patterned surfaces has been shown in Fig. 10(a). Directly after laser ablation, the WCAs declined dramatically and all the sample surfaces were highly hydrophilic. This phenomenon was well observed within 4 days after laser processing. It was unable to calculate WCAs since the water droplet almost completely penetrated into the grooves. The reason for this phenomenon was that the laser treated surface just after laser radiation was highly nonequilibrium, contained many surface defects and possessed a very high surface energy. Thus, this surface was characterized by the superhydrophilicity. 5 days later, the WCAs grew up gradually to arrive at 100°, which exhibited hydrophobic property. Beyond 15 days, except for the distance of 70 μm, the WCAs continued to increase and reach in the range of 130°-140°. Samples surfaces became much more hydrophobic. Beyond a certain period (20 days here), this increasing trend stopped. The steady WCA was noticed in the following days. All the WCAs reached to above 140° and the maximum WCA for line-patterned surface was 152.3 ± 1.2° with the RA of 8.8 ± 1.1°, which exhibited a superhydrophobic character. From Fig. 10(a), it also can be observed that the developments of WCA over time were different due to the various distance between the successive grooves on line patterned surfaces. Thus there were discrepancies for the final steady WCAs. It can be deduced that there is a possible link between surface roughness and the final steady WCA. Generally, the rougher surface was, the larger WCA was. In order to get desired surface with non-wetting character by laser texturing technique, the distance between

successive grooves should be selected reasonably.

The time evolutions of WCAs for grid-patterned and spot-patterned surfaces are shown in Fig. 10(b) and 10(c), respectively. Immediately after the laser treatment, WCAs for these two kinds of surfaces maintained at almost 0° for 4-5 days. After that, the values exhibited a significant increase trend to reach above 120°. Beyond a certain period (25 days here), the curves of WCA presented no major changes. For samples with grid pattern, except for distance of 60 μm, all the surfaces exhibited superhydrophobic character with the steady WCAs above 150° and RA below 10°. The maximum value even reached 156.8 ± 1.1° with the RA of just 6.5 ± 0.8°. Samples with spot pattern showed hydrophobic character with the contact angles above 90°. However, the maximum WCA was only 140.8 ± 2.8° and none RA was under 10°. Therefore, even after laser treatment, the spot-patterned surfaces cannot presente superhydrophobic property.

The results suggest that the changes of surface wettability can be related to the modification of surface topography. It can be explained either by Wenzel model [19] or by Cassie-Baxter model [20]. When the Wenzel's state occurs, the intrinsic surface wettability is enhanced by roughness: a hydrophilic surface becomes more hydrophilic with the growth of roughness, and a hydrophobic surface becomes more hydrophobic with an increase of roughness. Since the IN718 surface is initially hydrophilic, the performed nanosecond laser ablation would make it more hydrophilic with the smaller contact angle. In this study, it is well pronounced that the immediate improvement of hydrophilicity was observed at the first moments following laser treatment. That means the influence of surface topology was more preponderant and the Wenzel model was more likely.

However, the time dependency of WCA cannot be explained by surface morphology because surface microstructure did not change over time. Laser modified hydrophobic surfaces were reported elsewhere in previous literatures and the effect of surface chemistry seems more possible to explain such a change [42-43]. After laser treatment, the surface hydrophobicity gradually improved due to the possible change of surface chemical compositions. When the surface chemistry remained stable, the

constant WCAs were obtained. In this case, it is more likely that air pockets were trapped underneath the liquid droplet as described by Cassie-Baxter model，which contributed to the hydrophobic or superhydrophobic surfaces exhibiting the larger WCA and smaller RA.

3.3. Analysis of surface chemical composition

In order to verify above mentioned assumption, the elementary analysis of surface chemistry was carried out by XPS experiments when contact angles stabilized. The surface chemical compositions before and after laser irradiation were compared to evidence the possible effect of laser ablation on surface chemistry.

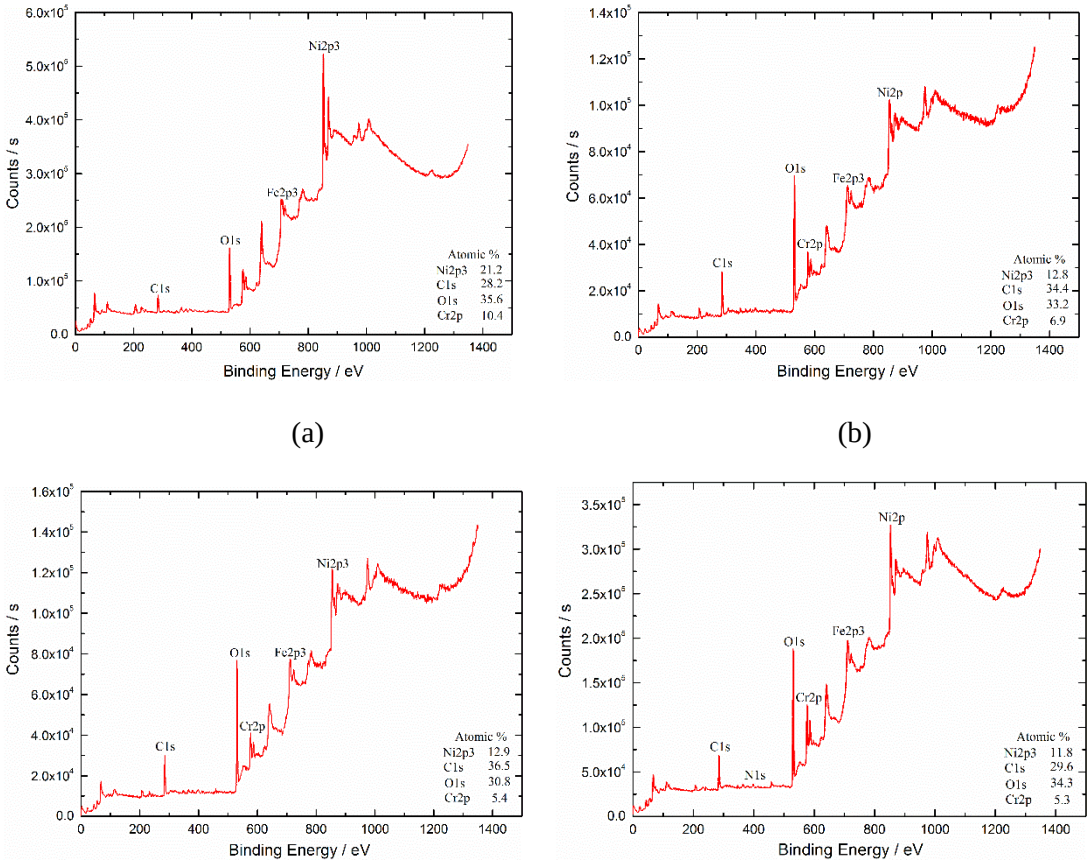

Figure 11. XPS spectra of IN718 surface (a) untreated surface (b) line pattern (c) grid pattern (d) spot pattern

The results of surface chemical compositions are shown in Fig. 11. Before laser treatment, the IN718 surface presented a carbon content of 28.2%, while after laser processing, the carbon content increased to 34.4%, 36.5%, and 29.6% for line pattern,

grid pattern, and spot pattern, respectively. The result indicates that after laser treatment a change in surface chemistry with the increase of carbon content clearly occurred. Thus, it can be verified from XPS analysis that the time dependency of surface wettability after laser treatment was due to the change of surface chemical compositions, especially the proportion of carbon content.

According to previous literature [39], although carbonization reaction and oxidation reaction would be inevitable to occur during laser processing since the experiments were conducted under the ambient air, the main reason why the laser treated surfaces exhibited superhydrophilic state just after the interaction between laser radiation and the substrate could be that such surface was highly nonequilibrium, contained a lot of surface defects and thus possessed a very high surface energy and was therefore characterized by the superhydrophilicity. For surface property, the wettability is highly sensitive to surface contaminations [44]. With the evolution of exposure time under ambient air, the original laser treated hydrophilic surfaces turned to be hydrophobic or superhydrophobic. Recentinvestigations show that the time dependency of surface wettability was related to the spontaneous adsorption of airborne hydrocarbon contaminations on the as-prepared surface [21, 39]. As a result, the proportion of carbon content on the surface would increase. Aria [45] and Liu [46] both have carried out independently further experiments in order to verify this conclusion. The surface chemistry was investigated by XPS for the samples with superhydrophobicity, before/after thermal annealing treatment, UV-O_3 treatment, and before/after Ar^+-etching in vacuum and re-exposure under ambient air [45-46].

In our work, the influence of surface morphology on wettability was formed directly after laser treatment and would not change over time. The time evolution of surface wettability of laser treated surfaces was attributed to the change of surface chemical compositions. Generally speaking, surface morphology and surface chemistry are the combined factors to obtain thermodynamically stable superhydrophobic surface on IN718 samples.

4. Conclusions

Experiments of nanosecond laser irradiation were carried out on IN718 surfaces

in the open air. In order to investigate surface morphology and surface wettability by laser treatment, three types of microstructures (line, grid and spot pattern) were fabricated on the samples surfaces. The results show that surface morphology and surface roughness can be controlled experimentally by varying surface pattern and laser parameters. These variations are accompanied by modifications of surface wettability. Directly after laser treatment, the contact angle declined dramatically and the surfaces became more hydrophilic, which can be explained by the Wenzel model. The WCAs of the laser treated surfaces witnessed a time dependency phenomenon due to the change of surface chemical compositions, especially the carbon content. As a result, several laser treated surfaces exhibited superhydrophobic property. We attributed the laser-induced change of the wetting behavior to the combined both surface morphology and surface chemical compositions.

Acknowledgements

The authors wish to acknowledge the technical supports of Tianjin University, University of Warwick, and Changchun University of Science and Technology. The authors are grateful for the financial support from National Natural Science Foundations of China [Nos.51405333, 51675371, 51675376 and 51675367], China-EU H2020 FabSurfWAR project (Nos.S2016G4501 and 644971), and the State Key Laboratory of Special Vehicles and Their Drive System Intelligent Manufacturing.

References:

[1] K. Venkatesan, R. Ramanujam, P. Kuppan, Parametric modeling and optimization of laser scanning parameters during laser assisted machining of Inconel 718, Opt. Laser Technol. 78 (2016) 10-18.

[2] K.H. Song, K. Nakata, Microstructural and mechanical properties of friction-stir-welded and post-heat-treated Inconel 718 alloy, J. Alloy. Compd. 505 (2010) 144-150.

[3] M. Anderson, R. Patwa, Y.C. Shin, Laser-assisted machining of Inconel 718 with an economic analysis, Int. J. Mach. Tools Manuf. 46 (2006) 1879-1891.

[4] Z. Wang, K. Guan, M. Gao, X. Li, X. Chen, X. Zeng, The microstructure and mechanical properties of deposited-IN718 by selective laser melting, J. Alloy.

Compd. 513 (2012) 518-523.

[5] H. Attia, S. Tavakoli, R. Vargas, V. Thomson, Laser-assisted high-speed finish turning of superalloy Inconel 718 under dry conditions, CIRP Ann-Manuf. Technol. 59 (2010) 83-88.

[6] Z.Y. Wang, K.P. Rajurkar, J. Fan, S. Lei, Y.C. Shin, G. Petrescu, Hybrid machining of Inconel 718, Int. J. Mach. Tools Manuf. 43 (2003) 1391-1396.

[7] B. Bhushan, Y.C. Jung, Natural and biomimetic artificial surfaces for superhydrophobicity, self-Cleaning, low adhesion, and drag reduction, Prog. Mater. Sci. 56 (2011) 1-108.

[8] Z. Yuan, J. Xiao, C. Wang, J. Zeng, S. Xing, J. Liu, Preparation of a superamphiphobic surface on a common cast iron substrate, J. Coat. Technol. Res. 8 (2011) 773-777.

[9] K. Ellinas, A. Tserepi, E. Gogolides, From superamphiphobic to amphiphilic polymeric surfaces with ordered hierarchical roughness fabricated with colloidal lithography and plasma nanotexturing, Langmuir 27 (2011) 3960-3969.

[10] K. Paso, T. Kompalla, N. Aske, H.P. Rønningsen, G. Øye, J. Sjoblom, Novel surfaces with applicability for preventing wax deposition: a review, J. Dispersion Sci. Technol. 30 (2009) 757-781.

[11] Y.C. Sheen, Y.C. Huang, C.S. Liao, H.Y. Chou, F.C. Chang, New approach to fabricate an extremely super-amphiphobic surface based on fluorinated silica nanoparticles, J. Polym. Sci. Part B: Polym. Phys. 46 (2008) 1984-1990.

[12] K. Liu, Y. Tian, L. Jiang, Bio-inspired superoleophobic and smart materials: design, fabrication, and application, Prog. Mater. Sci. 58 (2013) 503-564.

[13] C.T. Hsieh, J.M. Chen, R.R. Kuo, T.S. Lin, C.F. Wu, Influence of surface roughness on water- and oil-repellent surfaces coated with nanoparticles, Appl. Surf. Sci. 240 (2005) 318-326.

[14] V. Kumar, J. Pulpytel, H. Rauscher, I. Mannelli, F. Rossi, F.A. Khonsari, Fluorocarbon coatings via plasma enhanced chemical vapor deposition of 1H,1H,2H,2H-perfluorodecyl acrylate-2, morphology, wettability and antifouling characterization, Plasma Process. Polym. 7 (2010) 926-938.

[15] Z. Cui, L. Yin, Q. Wang, J. Ding, Q. Chen, A facile dip-coating process for preparing highly durable superhydrophobic surface with multi-scale structures on paint films, J. Colloid Interface Sci. 337 (2009) 531-537.

[16] S. Srinivasan, S.S. Chhatre, J.M. Mabry, R.E. Cohen, G.H. McKinley. Solution spraying of poly (methyl methacrylate) blends to fabricate microtextured, superoleophobic surfaces, Polymer 52 (2011) 3209-3218.

[17] K. Zhao, K.S. Liu, J.F. Li, W.H. Wang, L. Jiang. Superamphiphobic CaLi-based bulk metallic glasses, Scr. Mater. 60 (2009) 225-227.

[18] M. Psarski, J. Marczak, J. Grobelny, G. Celichowski, Superhydrophobic surface by replication of laser micromachined pattern in epoxy/alumina nanoparticle composite, J. Nanomater. 2 (2014) 105-119.

[19] R. N. Wenzel, Resistance of solid surfaces to wetting by water, J. Ind. Eng. Chem. 28 (1936) 988-994.

[20] A.B.D. Cassie, S. Baxter, Wettability of porous surfaces, Trans. Faraday Soc. 40 (1944) 546-551.

[21] L. B. Boinovich, A. M. Emelyanenko, A. S. Pashinin, C. H. Lee, J. Drelich, Y. K. Yap, Origins of thermodynamically stable superhydrophobicity of Boron Nitride nanotubes coatings, 28 (2012), 1206-1216.

[22] X. Yao, Y. L. Song, L. Jiang, Applications of bio-inspired special wettable surfaces, Adv. Mater. 23 (2013) 719-734.

[23] N. A. Ivanova, G. I. Rutberg, A. B. Philipchenko, Enhancing the superhydrophobic state stability of chitosan-based coatings for textiles, Macromol. Chem. Phys. 214 (2013), 1515-1521.

[24] D. Quéré, Non-sticking drops, Rep. Prog. Phys. 68 (2005) 2495-2532.

[25] Y.Q. Tang, Q. H. Zhang, X. L. Zhan, F. Q. Chen, Superhydrophobic and anti-icing properties at overcooled temperature of a fluorinated hybrid surface prepared via a sol-gel process, Soft Matter, 11 (2015) 4540-4550.

[26] Z. L. Jiang, S. Y. Fang, C. S. Wang, H. P. Wang, C. C. Ji, Durable polyorganosiloxane superhydrophobic films with a hierarchical structure by sol-gel and heat treatment method, Appl. Surf. Sci. 390 (2016) 993-1001.

[27] T. Hang, A. Hu, H. Ling, M. Li, D. Mao, Super-hydrophobic nickel films with micro-nano hierarchical structure prepared by electrodeposition, Appl. Surf. Sci. 256 (2010) 2400-2404.

[28] Y. Liu, X. Yin, J. Zhang, Y. Wang, Z. Han, L. Ren, L, Biomimetic hydrophobic surface fabricated by chemical etching method from hierarchically structured magnesium alloy substrate, Appl. Surf. Sci. 280 (2013) 845-849.

[29] N.G. Semaltianos, W. Perrie, P. French, M. Sharp, G. Dearden, K.G. Watkins, Femtosecond laser surface texturing of a nickelbased superalloy, Appl. Surf. Sci. 255 (2008) 2796-2802.

[30] B. Wu, M. Zhou, J. Li, X. Ye, G. Cai, Superhydrophobic surfaces fabricated by microstructuring of stainless steel using a femtosecond laser, Appl. Surf. Sci. 256 (2009) 61-66.

[31] G. Dumitru, V. Romano, Laser microstructuring of steel surfaces for tribological applications, Appl. Phys. A 70 (2000) 485-487.

[32] J. Li, L. Yan, H. Li, J. Li, F. Zha, Z. Lei, A facile one-step spray-coating process for the fabrication of superhydrophobic attapulgite coated mesh used in oil/water separation, RSC Adv. 5 (2015) 53802-53808.

[33] F. Mcklich, A.F. Lasagni, C. Daniel, Laser interference metallurgy-using interference as a tool for micro/nano structuring, Int. J. Mater. Res. 10 (2006) 1337-1344.

[34] L. B. Boinovich, A. M. Emelyanenko, A. D. Modestov, A. G. Domantovsky, K. A. Emelyanenko, Synergistic effect of superhydrophobicity and oxidized layers on corrosion resistance of aluminum alloy surface textured by nanosecond laser treatment, ACS Appl. Mater. Interfaces, 7 (2015) 19500-19508.

[35] T. C. Chen, H. T. Liu, H. F. Yang, W. Yan, W. Zhu, H. Liu. Biomimetic fabrication of robust self-assembly superhydrophobic surfaces with corrosion resistance properties on stainless steel substrate. RSC Adv. 6 (2016) 43937-43949.

[36] A. M. Emelyanenko, F. M. Shagieva, A. G. Domantovsky, L. B. Boinovich, Nanosecond laser micro- and nanotexturing for the design of asuperhydrophobic coating robust against long-term contact withwater, cavitation, and abrasion, Appl.

Sur. Sci. 332 (2015) 513-517.

[37] A. Milionis, D. Fragouli, F. Brandi, L. Liakos, S. Barroso, R. Ruffilli, A. Athanassiou, Superhydrophobic/superoleophilic magnetic elastomers by laserablation, Appl. Surf. Sci. 351 (2015) 74-82.

[38] D. V. Ta, A. Dunn, T. J. Wasley, R. W. Kay, J. Stringer, P. J. Smith, C. Connaughton, J. D. Shephard, Nanosecond laser textured superhydrophobic metallic surfaces and their chemical sensing applications. Appl. Surf. Sci. 357 (2015) 248-254.

[39] L. B. Boinovich, A. M. Emelyanenko, K. A. Emelyanenko, A. G. Domantovsky, A. A. Shiryaev, Comment on "Nanosecond laser textured superhydrophobic metallic surfaces and their chemical sensing applications" by Duong V. Ta, Andrew Dunn, Thomas J. Wasley, Robert W. Kay, Jonathan Stringer, Patrick J. Smith, Colm Connaughton, Jonathan D. Shephard (Appl. Surf. Sci. 357 (2015) 248-254), Appl. Surf. Sci. 379 (2016) 111-113.

[40] M.L. Wu, C.Z Ren, Active control of the anisotropic wettability of the carbon fiber reinforced carbon and silicon carbide dual matrix composites (C/C-SiC), Appl. Surf. Sci. 327 (2015) 424-431.

[41] C. Yang, X. Mei, Y. Tian, D. Zhang, Y. Li, X. Liu, Modification of wettability property of titanium by laser texturing, Int. J. Adv. Manuf. Technol. (2016) 1-8.

[42] A.M. Kietzig, M.N. Mirvakili, S. Kamal, P. Englezos, S.G. Hatzikiriakos, Cassie to Wenzel wetting transitions on femtosecond laser-patterned pure metallic substrates, J. Adhes. Sci. Technol. 25 (2011) 2789-2809.

[43] P. Bandoki, S. Valette, E. Audouard, S. Benayoun, Time dependency of the hydrophilicity and hydrophobicity of metallic alloys subjected to femtosecond laser irradiations, Appl. Surf. Sci. 273 (2013) 399-407.

[44] Z. T. Li, Y. J. Wang, A. Kozbial, G. Shenoy, F. Zhou, R. McGinley, P. Ireland, B. Morganstein, A. Kunkel, S. P. Surwade, L. Li, H. T.Liu, Effect of airborne contaminants on the wettability of supported graphene and graphite, Nat. Mater. 12 (2013) 1-7.

[45] A. I. Aria, P. R. Kidambi, R. S. Weatherup, L. Xiao, J. A. Williams, S. Hofmann, Time evolution of the wettability of supported graphene under ambient air

exposure, J. Phys. Chem. C 120 (2016) 2215-2224.

[46] P. Liu, L. Cao, W. Zhao, Y. Xia, W. Huang, Z. L. Li, Insights into the superhydrophobicity of metallic surfaces prepared by electrodeposition involving spontaneous adsorption of airborne hydrocarbons, Appl. Surf. Sci. 324 (2015) 576-583.